nature materials

ARTICLES

PUBLISHED ONLINE: 14 OCTOBER 2012 | DOI: 10.1038/NMAT3450

Bulk electronic structure of the dilute magnetic semiconductor $Ga_{1-x}Mn_xAs$ through hard X-ray angle-resolved photoemission

A. X. Gray[1,2,3]*, J. Minár[4], S. Ueda[5], P. R. Stone[2,6], Y. Yamashita[5], J. Fujii[7], J. Braun[4], L. Plucinski[8], C. M. Schneider[8], G. Panaccione[7], H. Ebert[4], O. D. Dubon[2,6], K. Kobayashi[5] and C. S. Fadley[1,2]

A detailed understanding of the origin of the magnetism in dilute magnetic semiconductors is crucial to their development for applications. Using hard X-ray angle-resolved photoemission (HARPES) at 3.2 keV, we investigate the bulk electronic structure of the prototypical dilute magnetic semiconductor $Ga_{0.97}Mn_{0.03}As$, and the reference undoped GaAs. The data are compared to theory based on the coherent potential approximation and fully relativistic one-step-model photoemission calculations including matrix-element effects. Distinct differences are found between angle-resolved, as well as angle-integrated, valence spectra of $Ga_{0.97}Mn_{0.03}As$ and GaAs, and these are in good agreement with theory. Direct observation of Mn-induced states between the GaAs valence-band maximum and the Fermi level, centred about 400 meV below this level, as well as changes throughout the full valence-level energy range, indicates that ferromagnetism in $Ga_{1-x}Mn_xAs$ must be considered to arise from both *p–d* exchange and double exchange, thus providing a more unifying picture of this controversial material.

Although the dilute ferromagnetic semiconductor system $Ga_{1-x}Mn_xAs$ has been known for some time[1–3], controversy still remains as to its electronic structure and the nature of the states producing ferromagnetic coupling[4–16]. Two extreme limits have been discussed for explaining ferromagnetism in these materials: that Mn strongly hybridizes with the GaAs valence bands and induces hole doping and magnetism through *p–d* exchange[4–7], or that Mn induces states that are split off from the valence band, and lie as an impurity band somewhere in the bandgap about 30–100 meV above the valence band maximum (VBM) leading to ferromagnetism through a double-exchange mechanism[8–15]. For example, very recent studies by resonant tunnelling spectroscopy and by a combination of ion scattering and X-ray techniques have concluded that such impurity bands control the interaction and can be tuned by varying dopant levels[14,15]. However, a recent theoretical overview suggests that both mechanisms can be active, particularly for $Ga_{1-x}Mn_xAs$ among the dilute magnetic semiconductors[16].

An essential element for better understanding the nature of the ferromagnetism in such dilute magnetic semiconductors is thus the direct measurement of the bulk valence electronic states, which, in principle, might be accessible by X-ray photoemission spectroscopy. However, a difficulty in obtaining such a direct measurement by conventional soft X-ray photoemission, which is very surface sensitive, has been that the preparation of the surface often destroys the crystallinity in the first few layers, and may also distort its stoichiometry. More specifically, etching of the sample, which has been widely accepted as an adequate surface preparation method[17,18], may not preserve the original structure and composition of the surface layers. Conventional angle-resolved photoemission spectroscopy (ARPES) with even lower photon energies of ~20–100 eV has been applied to this system[19], but at these energies, the measurement is even more surface sensitive owing to the short electron inelastic mean-free paths of about 3–6 Å (refs 20,21). Such shallow probing depths can lead to measurements for which surface effects dominate the spectra, and the true bulk electronic properties remain uncertain. There is thus a growing interest in performing ARPES measurements in the kiloelectronvolt[22] or even multi-kiloelectronvolt energy regime[23], to more quantitatively probe the true bulk properties of such materials. Hard X-ray ARPES (HARPES) has in fact recently been demonstrated in a study of the bulk electronic properties of W and GaAs using synchrotron radiation with photon energies of 6.0 and 3.2 keV, respectively[23]. In this study, we present a first true application of HARPES to investigate the electronic structure of $Ga_{1-x}Mn_xAs$ with $x = 0.03$ and a Curie temperature of ~100 K, as compared with that of pure GaAs. The experimental results are compared with the results of fully relativistic one-step model calculations for photoemission that include matrix-element effects and the alloy composition using the coherent potential approximation[24,25] (CPA).

The synthesis of our sample is described in the Methods, along with some details of our HARPES experimental procedure. The HARPES measurements were performed at a photon energy of 3.2 keV and 20 K, a temperature that is well below the Curie temperature of our sample of ~100 K. Sample cooling is

[1]Department of Physics, University of California Davis, Davis, California 95616, USA, [2]Materials Sciences Division, Lawrence Berkeley National Laboratory, Berkeley, California 94720, USA, [3]Stanford Institute for Materials and Energy Sciences, Stanford University and SLAC National Accelerator Laboratory, Menlo Park, California 94025, USA, [4]Department of Chemistry, Ludwig Maximillian University, 81377 Munich, Germany, [5]NIMS Beamline Station at SPring-8, National Institute for Materials Science, Hyogo 679-5148, Japan, [6]Department of Materials Science and Engineering, University of California Berkeley, Berkeley, California 94720, USA, [7]Istituto Officina dei Materiali IOM-CNR, Lab. TASC; S.S. 14 Km 163.5, in AREA Science Park, 34149 Trieste, Italy, [8]Peter Grünberg Institut PGI-6, Research Center Jülich, 52425 Jülich, Germany. *e-mail: axgray@slac.stanford.edu.

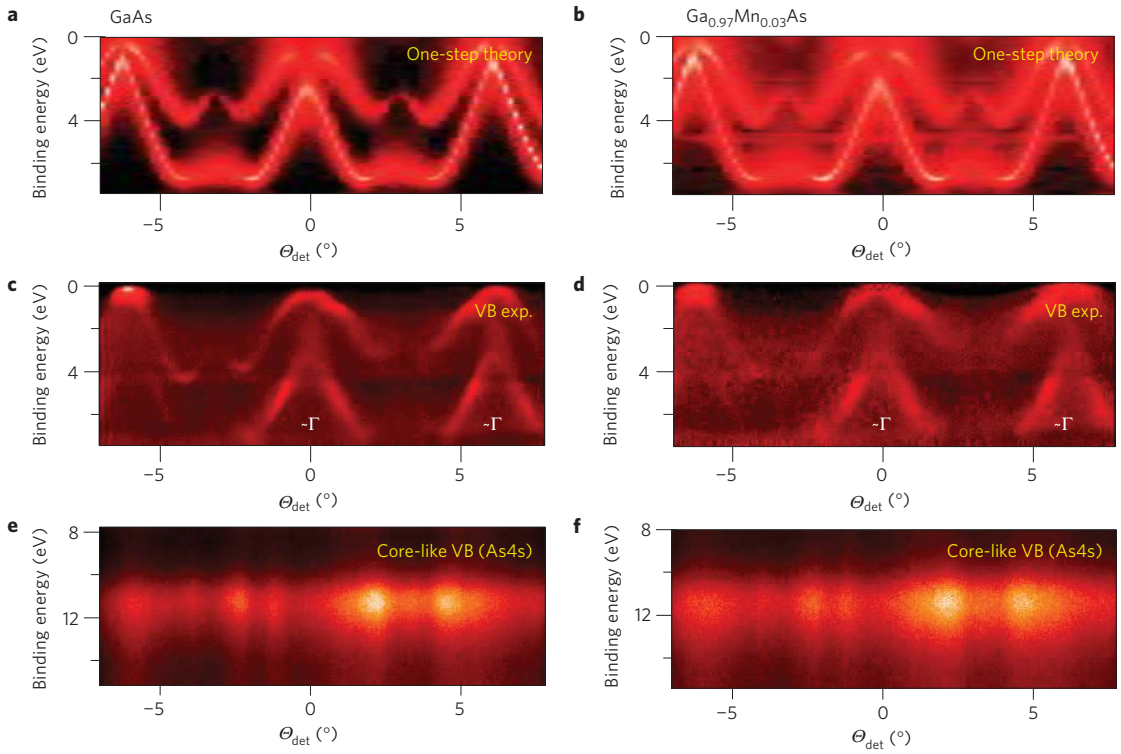

Figure 1 | HARPES measurements and one-step theory for bulk GaAs and $Ga_{0.97}Mn_{0.03}As$. a,**b**, Results of one-step HARPES calculations for GaAs (**a**) and $Ga_{0.97}Mn_{0.03}As$ (**b**). **c**,**d**, Experimental HARPES data obtained for GaAs (**c**) and $Ga_{0.97}Mn_{0.03}As$ (**d**). **e**,**f**, HARPES results for a mostly As 4*s* band at ~11 eV binding energy that is more core-like for the two materials, and exhibits similar characteristic XPD modulations for both. In **c** and **d**, the approximate positions of the repeated Γ points are indicated. VB, valence band.

also necessitated by the fact that, as discussed elsewhere[22,23], at higher energies and higher temperatures, spectral contributions due to phonon-assisted non-direct transitions smear out and suppress the dispersive direct-transition features associated with the band structure[26,27]. Such Brillouin-zone averaging thus limits the specification of the initial photoelectron wave vector, and is a key consideration in any HARPES experiment. At high enough photon energies and/or temperatures, this effect leads to the so-called X-ray photoemission spectroscopy (XPS) limit[28], in which measurement yields what is approximately a matrix-element weighted density of states (MEW-DOS) whose angular distributions now show X-ray photoelectron diffraction (XPD) effects[23,29]. As a further approximation, atomic differential cross-sections can be used to weight element-projected DOS, as we discuss briefly below. The extent of the phonon smearing can be approximately quantified using a photoemission Debye–Waller factor, which predicts the fraction of the direct transitions in a solid for a given photon energy and temperature, and is given by $W(T) = \exp[-(1/3)g_{hlk}^2\langle U^2(T)\rangle]$, where g_{hlk} is the magnitude of the bulk reciprocal-lattice vector involved in the direct transitions for a given photon energy and $\langle U^2(T)\rangle$ is the three-dimensional mean-squared vibrational displacement for a given temperature[26–28]. Therefore, even at high photon energies, the effects of phonon smearing can be mitigated by means of cooling the sample to low temperatures. As an example, at a photon energy of 3.2 keV and sample temperature of 300 K, the fraction of direct transitions in GaAs is estimated to be less than 5%, which means that over 95% of the angle-resolved photoemission signal is going to be influenced by phonon smearing and spectra will be dominated by MEW-DOS features. However, by cryogenically cooling the sample to 20 K, we increase the fraction of direct transitions in the solid to over 30% (ref. 22), which should result in a clearer definition of the dispersive bands on top of the DOS-like background, therefore enabling a bulk band-structure study of GaAs and $Ga_{0.97}Mn_{0.03}As$, as demonstrated already for undoped GaAs (ref. 23).

The reciprocal-space geometry of the experiment is shown in Figure 1b of ref. 23, in an extended Brillouin-zone picture. The final state is assumed in this picture to be a free electron, a very good assumption for this high 3.2 keV energy. The magnitude of the final photoelectron wave vector $\mathbf{k}_f$ can be calculated using $E_f(\mathbf{k}_f) \approx \hbar^2 k_f^2/2m_e$, where E_f is the electron kinetic energy inside the surface and m_e is the electron mass. As the dipole approximation no longer fully holds in the hard X-ray regime[23,27], the magnitude and direction of the final photoelectron wave vector $\mathbf{k}_f$ have to be adjusted by the photon wave vector $-\mathbf{k}_{h\nu}$, according to the simple wave vector conservation equation $\mathbf{k}_i = \mathbf{k}_f - \mathbf{k}_{h\nu} - \mathbf{g}_{hk\ell}$. As a result of taking the photon momentum into account, the central location of our angular measurement window in the extended Brillouin zone shifts for our geometry by 3.0° in the direction perpendicular to $\mathbf{k}_f$, because of the 90° angle between the photon incidence and the photoemission direction, and ends up near the Γ point. In our particular case, the detector spans ~ 15° of the arc, so that our measurement, centred approximately at the Γ point in the Brillouin zone, traverses the distance from Γ to K to U to X about three times. Thus, a single HARPES detector image will show several cross-sections of the Brillouin zone[22,23].

In Fig. 1 we compare the results of fully relativistic one-step theory of photoemission calculations that include matrix-element effects for GaAs in Fig. 1a and $Ga_{0.97}Mn_{0.03}As$ in Fig. 1b to the corresponding experimental valence-band HARPES data in Fig. 1c,d, respectively. The experimental valence-band spectra have been normalized by energy- and angle-averaged curves to minimize the effects of DOS and XPD modulations across the detector image, as discussed elsewhere[22,23]. Such normalization is expected to remove the constant-angle (MEW-DOS) and constant-energy (XPD) modulations from the detector image, thus optimally

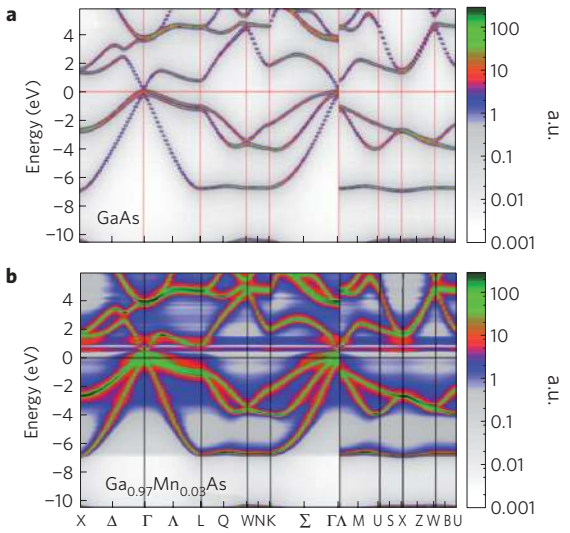

Figure 2 | One-step theory spectral functions for GaAs and $Ga_{0.97}Mn_{0.03}As$. a,**b**, Spectral functions (band structures) used for the HARPES simulations and calculated for GaAs (**a**) and $Ga_{0.97}Mn_{0.03}As$ (**b**).

emphasizing the dispersive bands (A. Bostwick and E. Rotenberg, private communication). The calculations agree very well with the experimental data. As expected from the extended Brillouin-zone picture[23], the Γ–K/U–X–K/U–Γ region is repeated about three times in the detector image, which spans about 15° of the arc traversed by the vector $\mathbf{k}_f - \mathbf{k}_{h\nu}$. The first major difference between the GaAs and $Ga_{0.97}Mn_{0.03}As$ electronic structures observed in the experiment and confirmed by the theory is the smearing of the band features in $Ga_{0.97}Mn_{0.03}As$ as compared with GaAs: this is at least partly due to the presence of the Mn impurities that disturb the long-range translational order of the host GaAs crystal. Figure 2a,b also shows this very clearly from a theoretical perspective, in comparing the predicted spectral function of GaAs with that of $Ga_{0.97}Mn_{0.03}As$, as calculated within CPA. The calculations for $Ga_{0.97}Mn_{0.03}As$ are considerably broadened over the entire Brillouin zone, as compared with the clean and sharp dispersive bands for pure GaAs.

Consistent with previous HARPES measurements of GaAs (ref. 23), we observe a lack of dispersion for a feature at ∼11–12 eV below the VBM, for both GaAs and $Ga_{0.97}Mn_{0.03}As$ (Fig. 1e,f). This band is largely As 4*s* in character and thus highly localized; thus, its angular distribution is more core-like and exhibits intensity modulations with detector angle that are characteristic of core-level XPD; these are essentially identical in form for both GaAs and $Ga_{0.97}Mn_{0.03}As$, as expected because XPD will probe only the local atomic structure around As, which is little perturbed by the presence of the Mn dopant.

In Fig. 3, we now compare the experimental angle-integrated valence-band spectra for GaAs and $Ga_{0.97}Mn_{0.03}As$ from Fig. 1c,d to analogous theoretical spectra obtained using the one-step CPA calculations, which included a complete angle integration. Such angle-integration should lead to results reflecting the MEW-DOS. The experimental valence-band spectra were normalized to the intensities of the As 3*s* core levels, which should be the same

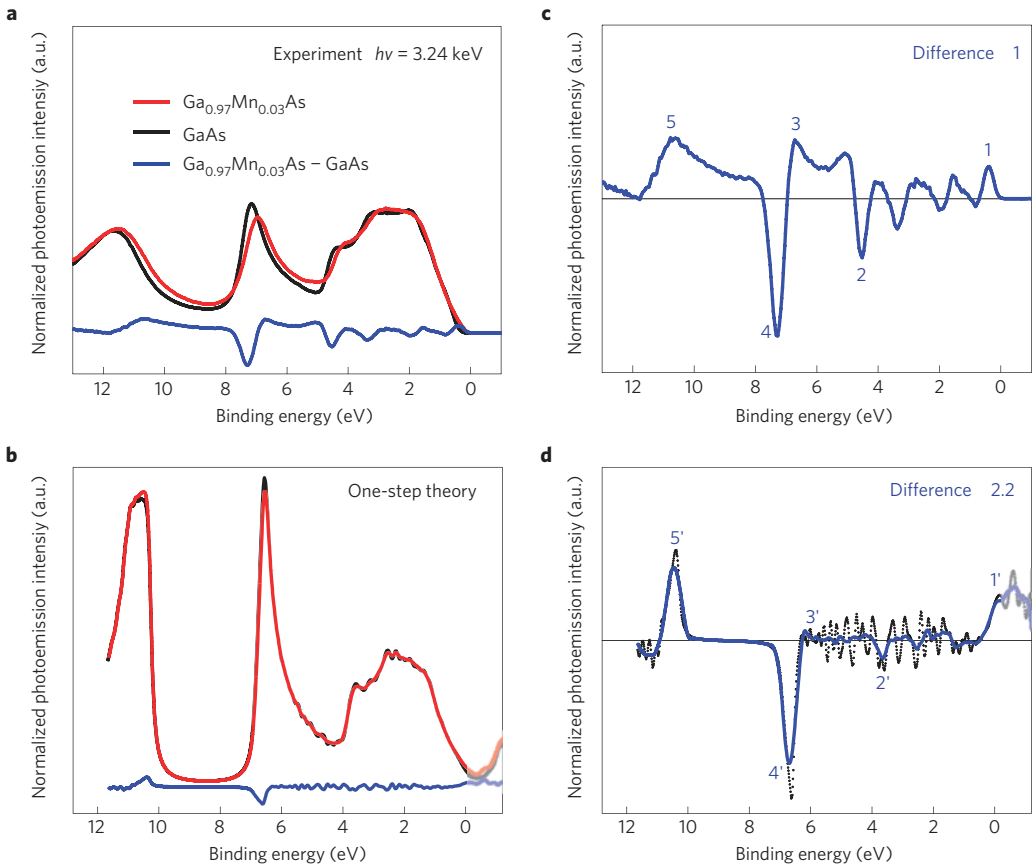

Figure 3 | Angle-integrated valence-band spectra for GaAs and $Ga_{0.97}Mn_{0.03}As$. a, Experimental angle-integrated valence-band spectra for GaAs and $Ga_{0.97}Mn_{0.03}As$. **b**, Theoretical spectra obtained using one-step theory calculations. **c**,**d**, Intensity difference spectra between $Ga_{0.97}Mn_{0.03}As$ and GaAs for the experimental data (**c**) and the one-step theory results (**d**). The theoretical difference has been multiplied by 2.2 to permit more direct comparison with experiment.

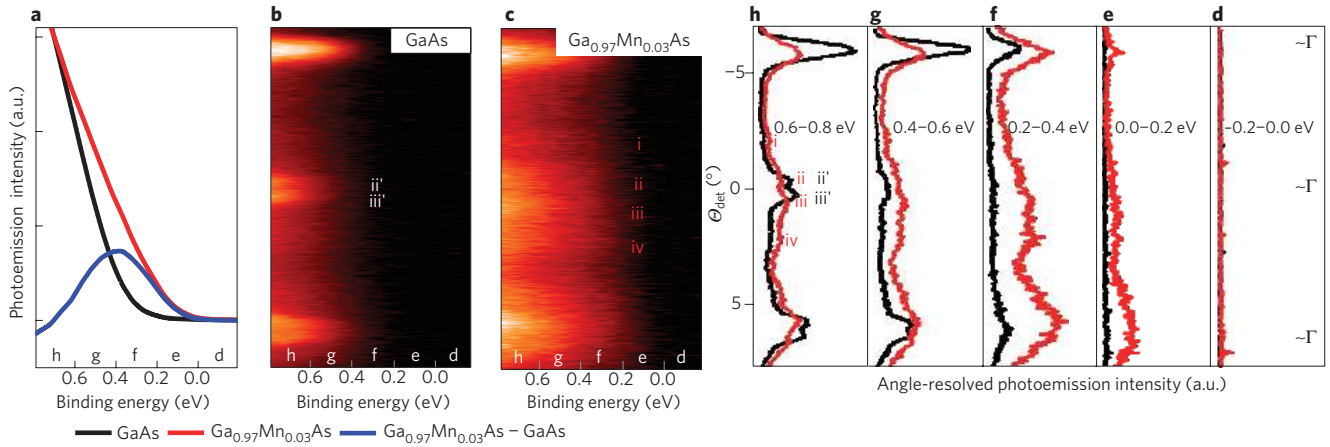

Figure 4 | Analysis of the near-Fermi-edge region in the HARPES data. a, A blow-up of the angle-integrated GaAs and GaMnAs spectra and difference over the 1.0 eV interval spanning the −0.2 − 0.8 binding energy shown in Fig. 3a. **b**,**c**, Angle-resolved data as a function of detector angle over the same energy range as shown in **a**, for both materials. Fine structure features are noted by ii′ and iii′ for GaAs and i, ii, iii and iv for $Ga_{0.97}Mn_{0.03}As$. **d**–**h**, Angle-resolved data integrated over the successive 0.2 eV binding energy intervals of **a**–**c**, with the black curves for GaAs and the red curves for $Ga_{0.97}Mn_{0.03}As$. Again, the approximate positions of repeated Γ points are indicated.

for both GaAs and $Ga_{0.97}Mn_{0.03}As$, because the As atoms are not substituted by Mn during the implantation. All of the major features in the experimental spectra (Fig. 3a) are well reproduced by the theory (Fig. 3b), with the exception of the overestimated relative intensity and sharpness of the features at 6.5 eV and 11 eV in theory, which is probably caused in experiment by the combined effects of total experimental resolution (including decreased lifetime as the binding energy increases), and residual disorder-induced broadening, as seen recently in a CrAl alloy[30].

We also show intensity difference plots ($Ga_{0.97}Mn_{0.03}As$–GaAs) in Fig. 3, with expanded views in Fig. 3c,d. The raw theoretical difference spectrum in Fig. 3d, shown with black dots, exhibits fine peaks with widths that are much smaller than the instrumental resolution (250 meV). Therefore, for a fair comparison, we also show in Fig. 3d, as the solid blue curve, a theoretical difference for which a Gaussian broadening of 250 meV is applied to approximately account for the total instrumental resolution. We have also labelled the main features in the difference plots 1–5 (experiment) and 1′–5′ (theory). Theoretical results for binding energies above 0 eV are dimmed, because equivalent experimental data do not exist for these unoccupied states. In general, there is excellent agreement between experiment and theory for these difference plots, with all of features 1–5 showing theoretical counterparts 1′–5′. Although the theoretical differences are smaller by about a factor of 2.2, this could well be due to less angular averaging over our detector window as compared with the complete averaging in theory, and the degree of agreement nonetheless indicates an accurate and consistent theoretical description of the valence electronic structure of this dilute magnetic semiconductor. These results thus also indicate that Mn induces subtle changes in the electronic structure, including peak shifts and changes in shape, over the entire valence manifold, including even the more localized As 4*s*-dominated band associated with peaks 5 and 5′. Such peak shifts have in fact been discussed in a previous local density approximation (LDA) study[31].

However, the most striking feature of these experimental data, which is also confirmed by the calculations, is the emergence of features 1 and 1′ above the VBM, which provide a clear signature of the Mn-induced states that are thought in the impurity-band model to be responsible for the magnetic coupling. This finding is also consistent with the more surface-sensitive previous ARPES study, which identified a rather flat band at about 0.2 eV below the Fermi energy[19]. The full-width at half-maximum of experimental feature 1 is 350 meV, which implies through square addition involving the 250 meV experimental resolution that its inherent width is about 240 meV, and thus significantly above the 30–100 meV separation proposed in some discussions of the impurity-band model (for example, ref. 14). This region 1 in experiment is shown in a magnified version in Fig. 4a, again with the difference in blue. To further investigate this near-Fermi-level region for experiment in an angle-resolved representation, we have divided the 1-eV-wide region between −0.2 (above E_F) and +0.8 eV in Fig. 4a, which is shown in angle-resolved form in Fig. 4b,c for the two materials, into five equal 0.2 eV sections labelled d–h and examined them for both GaAs and $Ga_{0.97}Mn_{0.03}As$. Intensities have as before been normalized to As 3*s*. First, one notices from Fig. 4b,c that the presence of Mn induces intensity in the angle-resolved spectra that is 0.2–0.3 eV above that for GaAs, and that this intensity shows a different dispersion, being not only broader, but with additional and different features labelled i (weaker), ii, iii and iv that are different from ii′ and iii′ for GaAs. Integrating the intensity over angle in each of the five energy intervals leads to the curves for the two materials shown in Fig. 4d–h. The onset of photoemission intensity due to the Mn states is evident in Fig. 4e corresponding to the binding-energy range between 0 and 0.2 eV. The Mn-derived feature continues to grow over the binding-energy range between 0.2 and 0.6 eV, as shown in Fig. 4g–f. Finally, in Fig. 4h, the angle-integrated photoemission intensities for GaAs and $Ga_{0.97}Mn_{0.03}As$ reach comparable values in the binding-energy range between 0.6 and 0.8 eV, as is also evident from the near-zero difference value in Fig. 4a; however, there is still a difference in the features ii′ and iii′ and i, ii, iii and iv that are observed. Also, as noted above, the angle-resolved spectra in the binding-energy range shown in Fig. 4g,h still exhibit major differences, with sharper and stronger GaAs bands, and smeared-out $Ga_{0.97}Mn_{0.03}As$ bands nevertheless still dominating the regions between the GaAs bands owing to the presence of the Mn-induced states. It is important to note that neither the angle-integrated spectra nor the angle-resolved HARPES maps show any kind of clear separation or even intensity drop near E_F that would indicate the presence of a gap between the valence bands and a Mn impurity band[14], even if we allow for the present experimental energy resolution of ∼250 meV, as discussed above in connection with feature 1. This clearly indicates that the tail of the impurity band is merged with the GaAs valence bands, as for example suggested in refs 4–7, including experimental results from d.c. transport and optical properties measurements

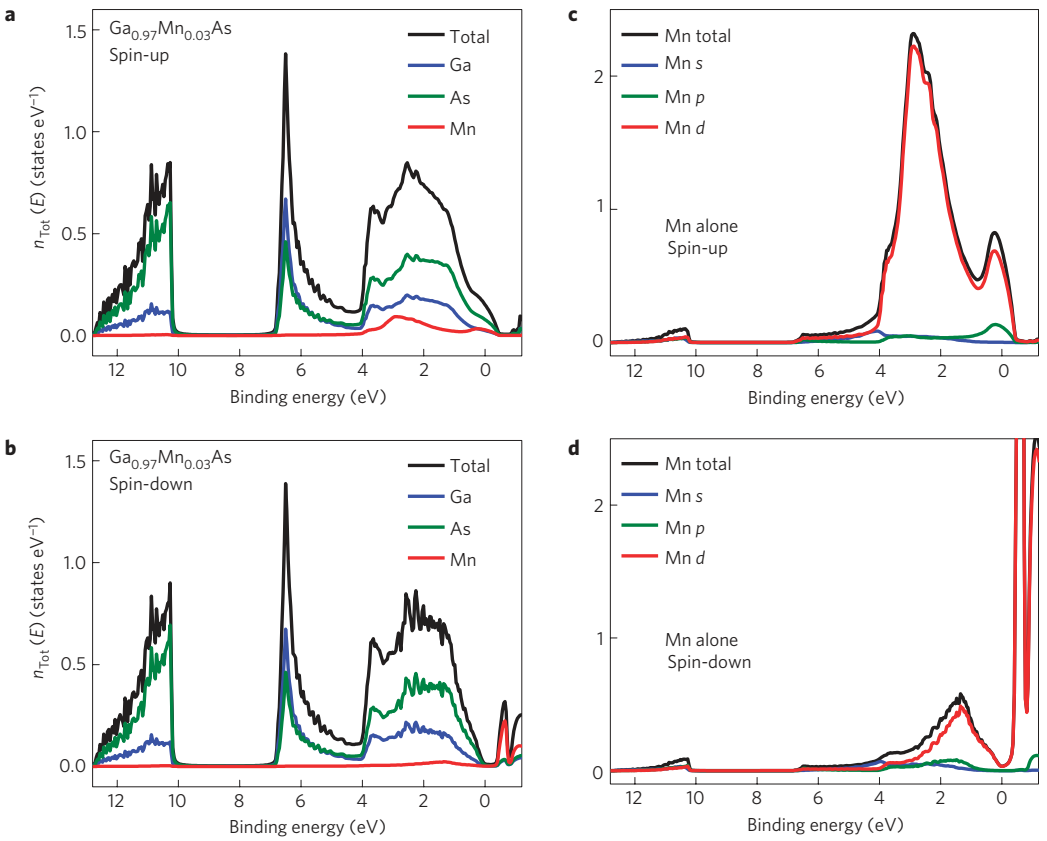

Figure 5 | GaAs and $Ga_{0.97}Mn_{0.03}$ As theoretical DOS. a,**b**, Calculated spin-resolved element- and orbital-projected DOS for $Ga_{0.97}Mn_{0.03}As$, with Ga, As and Mn contributions indicated. **c**,**d**, Calculated spin-resolved projected DOS for Mn alone in $Ga_{0.97}Mn_{0.03}As$, with *s*, *p* and *d* contributions indicated.

in ref. 4, although not by a recent resonant tunnelling study[14]. On the other hand, our results are qualitatively consistent with another recent study, in providing evidence for Mn-induced states overlapping the Fermi level[15].

As a final point, we turn again to theory, and in Fig. 5 show DOS for ferromagnetically ordered $Ga_{0.97}Mn_{0.03}As$ calculated using the same CPA LDA model as for the one-step photoemission process of Figs 1a,b, 2 and 3b,d. Results are shown for both spin-up (Fig. 5a,c) and spin-down (Fig. 5b,d), and the different Mn components are shown on an expanded scale in Fig. 5c,d, with the results in Fig. 5c,d for Mn 3*d* also being in excellent agreement with a previous LDA study for the lower-binding energy region[31]. These results make it clear that Mn 3*d*, almost entirely spin-up in the ferromagnetic state, contributes significantly to the electronic structure from the Fermi level (where it is ~20%, with ~60% contribution from Ga and ~20% from As) to about 4 eV binding energy, with the spin-up contribution of course lying at higher binding energies owing to the assumed ferromagnetic state. Further considering the relative atomic photoelectric cross-sections per electron for Mn 3*d*, Mn 4*s*, Ga 4*p* and As 4*p* (ref. 32), which are in a ratio 1.0:5.2:5.4:6.4, respectively, further indicates that our peak 1 should predominantly reflect Mn $3d+4s$ and Ga 4*p* contributions. Improving on the electronic structure model by incorporating a correlation correction using LDA+*U* is expected to increase the binding energies of the 3*d* states[33], enhancing the degree of overlap of the Mn impurity bands with the GaAs valence bands.

We have used HARPES to study the differences between the bulk electronic structures of a parent semiconductor GaAs and a dilute ferromagnetic semiconductor derived from it, $Ga_{1-x}Mn_xAs$ with $x=0.03$. Clear differences between the electronic structures of GaAs and $Ga_{0.97}Mn_{0.03}As$ were observed, including smearing of the sharp band features, changes throughout the entire valence-band manifold, and the appearance of extra intensity at the VBM that extends up to the Fermi level. These changes are furthermore in excellent agreement with one-step photoemission theory. A further analysis of angle-resolved data near the VBM indicates additional states induced by Mn over roughly 0–0.4 eV binding energy. Finally, element- and orbital-projected DOS calculations are consistent with theory in showing significant Mn contributions over the 0–4 eV binding energy, and particularly near E_F. Our results thus strongly favour a model of $Ga_{1-x}Mn_xAs$ in which there is no gap between the Mn-induced impurity band and the GaAs valence bands, with this band being centred about 400 meV below and weakly overlapping the Fermi level, and by implication suggest that the magnetism originates from the coexistence of the two different mechanisms discussed in previous papers—double exchange and *p*–*d* exchange, as recently suggested on the basis of theory[16].

Methods

$Ga_{1-x}Mn_xAs$ was synthesized using a combination of ion implantation and pulsed-laser melting, details of which can be found elsewhere[34,35]. Briefly, 50 keV Mn^+ ions were implanted into a piece of semi-insulating GaAs(001) wafer to a dose of 1.5×10^{16} cm^{-2}, followed by irradiation with a single pulse from a KrF ($\lambda=248$ nm) excimer laser at a fluence of ~ 0.3 J cm^{-2}. Samples were etched in concentrated HCl for 20 min to remove a very thin highly defective surface layer as well as any surface oxide phases[34,36]. These processing conditions give rise to a $Ga_{1-x}Mn_xAs$ film that is approximately 100 nm thick and with $x\approx0.03$ (ref. 37). Temperature-dependent magnetization measurements in a superconducting quantum interference device magnetometer indicate that the Curie temperature (T_C) of the $Ga_{1-x}Mn_xAs$ film is ~100 K. Before the HARPES measurements the samples were again briefly etched in concentrated HCl and immediately placed under vacuum to minimize the effects of Mn-related oxides, which have previously been shown to interfere with electron-yield-based X-ray spectroscopy[36].

The HARPES measurements were performed at undulator beamline BL15XU (ref. 38) of the SPring-8 facility. The photon energy was set to 3,241.2 eV. At this energy, the inelastic mean-free path of $Ga_{0.97}Mn_{0.03}As$ is estimated to be ~57 Å (refs 20,21), and the measurement should thus be ~10–20 times more

bulk sensitive compared with conventional ARPES in the 20–100 eV range[19]. The experimental geometry is shown in Figure 2 of ref. 23. The angle of incidence was fixed at 2° as measured from the sample surface, and the photoelectron take-off angle was fixed at 90° with respect to the X-ray incidence angle, or equivalently at 2° as measured from the sample normal. The photoemitted electrons were analysed for their kinetic energy and angle of emission using a VG Scienta R4000 hemispherical analyser. The experimental energy resolution was determined to be ~250 meV, using a Au Fermi edge measurement.

The fully relativistic one-step model of photoemission calculations is based on the multiple scattering KKR band structure method[24,25].

Received 31 October 2011; accepted 10 September 2012; published online 14 October 2012

References

1. Ohno, H. *et al.* (Ga, Mn)As: A new diluted magnetic semiconductor based on GaAs. *Appl. Phys. Lett.* **69,** 363–365 (1996).
2. Ohno, H. Making nonmagnetic semiconductors ferromagnetic. *Science* **281,** 951–956 (1998).
3. Ohno, Y. *et al.* Electrical spin injection in a ferromagnetic semiconductor heterostructure. *Nature* **402,** 790–792 (1999).
4. Dietl, T., Ohno, H., Matsukura, F., Cibert, J. & Ferrand, D. Zener model description of ferromagnetism in zinc-blende magnetic semiconductors. *Science* **287,** 1019–1022 (2000).
5. Dietl, T., Ohno, H. & Matsukura, F. Hole-mediated ferromagnetism in tetrahedrally coordinated semiconductors. *Phys. Rev. B* **63,** 195205 (2001).
6. Mašek, J. *et al.* Microscopic analysis of the valence band and impurity band theories of (Ga, Mn)As. *Phys. Rev. Lett.* **105,** 227202 (2010).
7. Neumaier, D. *et al.* All-electrical measurement of the density of states in (Ga, Mn)As. *Phys. Rev. Lett.* **103,** 087203 (2009).
8. Hirakawa, K., Katsumoto, S., Hayashi, T., Hashimoto, Y. & Iye, Y. Double-exchange-like interaction in $Ga_{1-x}Mn_xAs$ investigated by infrared absorption spectroscopy. *Phys. Rev. B* **65,** 193312 (2002).
9. Burch, K. S. *et al.* Impurity band conduction in a high temperature ferromagnetic semiconductor. *Phys. Rev. Lett.* **97,** 087208 (2006).
10. Sapega, V. F., Moreno, M., Ramsteiner, M., Däweritz, L. & Ploog, K. H. Polarization of valence band holes in the (Ga, Mn)As diluted magnetic semiconductor. *Phys. Rev. Lett.* **94,** 137401 (2005).
11. Ando, K., Saito, H., Agarwal, K. C., Debnath, M. C. & Zayets, V. Origin of the anomalous magnetic circular dichroism spectral shape in ferromagnetic $Ga_{1-x}Mn_xAs$: Impurity bands inside the band gap. *Phys. Rev. Lett.* **100,** 067204 (2008).
12. Rokhinson, L. P. *et al.* Weak localization in $Ga_{1-x}Mn_xAs$: Evidence of impurity band transport. *Phys. Rev. B* **76,** 161201(R) (2007).
13. Alberi, K. *et al.* Formation of Mn-derived impurity band in III-Mn-V alloys by valence band anticrossing. *Phys. Rev. B* **78,** 075201 (2008).
14. Ohya, S., Takata, K. & Tanaka, M. Nearly non-magnetic valence band of the ferromagnetic semiconductor GaMnAs. *Nature Phys.* **7,** 342–347 (2011).
15. Dobrowolska, M. *et al.* Controlling the Curie temperature in (Ga, Mn)As through location of the Fermi level within the impurity band. *Nature Mater.* **11,** 444–449 (2012).
16. Sato, K. *et al.* First-principles theory of dilute magnetic semiconductors. *Rev. Mod. Phys.* **82,** 1633–1690 (2010).
17. Edmonds, K. W. *et al.* High-Curie-temperature $Ga_{1-x}Mn_xAs$ obtained by resistance-monitored annealing. *Appl. Phys. Lett.* **81,** 4991–4993 (2002).
18. Olejník, K. *et al.* Enhanced annealing, high Curie temperature, and low-voltage gating in (Ga, Mn)As: A surface oxide control study. *Phys. Rev. B* **78,** 054403 (2008).
19. Okabayashi, J. *et al.* Angle-resolved photoemission study of $Ga_{1-x}Mn_xAs$. *Phys. Rev. B* **64,** 125304 (2001).
20. Powell, C. J., Jablonski, A., Tilinin, I. S., Tanuma, S. & Penn, D. R. Surface sensitivity of Auger-electron spectroscopy and X-ray photoelectron spectroscopy. *J. Electron Spectrosc. Relat. Phenom.* **98,** 1–15 (1999).
21. Tanuma, S., Powell, C. J. & Penn, D. R. Calculations of electron inelastic mean free paths. IX. Data for 41 elemental solids over the 50 eV to 30 keV range. *Surf. Interface Anal.* **43,** 689–713 (2011).
22. Papp, C. *et al.* Band mapping in X-ray photoelectron spectroscopy: An experimental and theoretical study of W(110) with 1.25 keV excitation. *Phys. Rev. B* **84,** 045433 (2011).
23. Gray, A. X. *et al.* Probing bulk electronic structure with hard X-ray angle-resolved photoemission. *Nature Mater.* **10,** 759–764 (2011).
24. Braun, J., Minár, J., Ebert, H., Katsnelson, M. I. & Lichtenstein, A. I. Spectral function of ferromagnetic 3*d* metals: A self-consistent LSDA+DMFT approach combined with the one-step model of photoemission. *Phys. Rev. Lett.* **97,** 227601 (2006).
25. Braun, J., Minár, J., Matthes, F., Schneider, C. M. & Ebert, H. Theory of relativistic photoemission for correlated magnetic alloys: LSDA+DMFT study of the electronic structure of Ni_xPd_{1-x}. *Phys. Rev. B* **82,** 024411 (2010).
26. Shevchik, N. J. Disorder effects in angle-resolved photoelectron spectroscopy. *Phys. Rev. B* **16,** 3428–3442 (1977).
27. Hussain, Z., Fadley, C. S. & Kono, S. Temperature-dependent angle-resolved X-ray photoemission study of the valence bands of single-crystal tungsten: Evidence for direct transitions and phonon effects. *Phys. Rev. B* **22,** 3750–3766 (1980).
28. Fadley, C. S. X-ray photoelectron spectroscopy: Progress and perspectives. *J. Electron Spectrosc. Relat. Phenom.* **178–179,** 2–32 (2010).
29. Vincente Alvarez, M. A., Ascolani, H. & Zampieri, G. Excitation of phonons and forward focusing in X-ray photoemission from the valence band. *Phys. Rev. B* **54,** 14703–14712 (1996).
30. Boekelheide, Z. *et al.* Band gap and electronic structure of an epitaxial, semiconducting $Cr_{0.80}Al_{0.20}$ thin film. *Phys. Rev. Lett.* **105,** 236404 (2010).
31. Sato, K., Dederichs, P. H., Katayama-Yoshida, H. & Kudrnovsky, J. Exchange interactions in diluted magnetic semiconductors. *J. Phys. Condens. Matter* **16,** S5491–S5497 (2004).
32. Trzhaskovskaya, B., Nefedov, V. I. & Yarzhemsky, V. G. Photoelectron angular distribution parameters for elements Z = 55 to Z = 100 in the photoelectron energy range 100–5000 eV. *Atom. Data Nucl. Data Tables* **82,** 257–311 (2002).
33. Sato, K., Dederichs, P. H. & Katayama-Yoshida, H. Curie temperatures of dilute magnetic semiconductors from LDA+U electronic structure calculations. *Physica B* **376–377,** 639–642 (2006).
34. Dubon, O. D., Scarpulla, M. A., Farshchi, R. & Yu, K. M. Doping and defect control of ferromagnetic semiconductors formed by ion implantation and pulsed-laser melting. *Physica B* **376,** 630–634 (2006).
35. Scarpulla, M. A. *et al.* Ferromagnetic $Ga_{1-x}Mn_xAs$ produced by ion implantation and pulsed-laser melting. *Appl. Phys. Lett.* **82,** 1251–1253 (2003).
36. Edmonds, K. W. *et al.* Surface effects in Mn $L_{3,2}$ X-ray absorption spectra from (Ga, Mn)As. *Appl. Phys. Lett.* **84,** 4065–4067 (2004).
37. Scarpulla, M. A. *et al.* Electrical transport and ferromagnetism in $Ga_{1-x}Mn_xAs$ synthesized by ion implantation and pulsed-laser melting. *J. Appl. Phys.* **103,** 073913 (2008).
38. Ueda, S. *et al.* Present status of the NIMS contract beamline BL15XU at SPring-8. *AIP Conf. Proc.* **1234,** 403–406 (2010).

Acknowledgements

This work was funded by the US Department of Energy under Contract No. DE-AC02-05CH11231, including salary and travel support for C.S.F. and A.X.G. The authors are grateful to HiSOR, Hiroshima University and JAEA/SPring-8 for the development of HXPS at BL15XU of SPring-8. The experiments at BL15XU were performed under the approval of NIMS Beamline Station (Proposal No. 2009A4906). This work was partially supported by the Nanotechnology Network Project, MEXT, Japan. Research at Stanford was supported through the Stanford Institute for Materials and Energy Science and the LCLS by the US Department of Energy, Office of Basic Energy Sciences. Financial support from German funding agencies DFG (SFB 689, EB 154/18 and EB 154/20) and the German ministry BMBF (05K10WMA) is also gratefully acknowledged (J.M., J.B. and H.E.).

Author contributions

A.X.G. and S.U. carried out the experiments, with assistance from Y.Y. and under the supervision of K.K. and C.S.F. Data normalization and analysis were performed by A.X.G and under the supervision of C.S.F. Theoretical calculations were carried out by J.M. J.B. and H.E. (one-step theory), and by L.P. with support from C.M.S. (additional free-electron final-state theory band structure). Samples were grown by P.R.S. under the supervision on O.D.D. Additional supporting measurements were carried out by J.F. under the supervision of G.P.

Additional information

Reprints and permissions information is available online at www.nature.com/reprints. Correspondence and requests for materials should be addressed to A.X.G.

Competing financial interests

The authors declare no competing financial interests.